# Electron delocalization and relaxation behavior in Cu-doped $Bi_2Se_3$ films

Mingze Li,[1] Zhenhua Wang,[1,*] Liang Yang,[1] Da Li,[1] Q. R. Yao,[2] G. H. Rao,[2] Xuan P. A. Gao,[3] and Zhidong Zhang[1,†]

[1]*Shenyang National Laboratory for Materials Science, Institute of Metal Research, Chinese Academy of Sciences, and School of Materials Science and Engineering, University of Science and Technology of China, 72 Wenhua Road, Shenyang 110016, China*

[2]*Guangxi Key Laboratory of Information Materials, School of Material Science and Engineering, Guilin University of Electronic Technology, 1 Jinji Road, Guilin, Guangxi 541004, China*

[3]*Department of Physics, Case Western Reserve University, Cleveland, Ohio 44106, USA*

(Received 22 February 2017; revised manuscript received 18 July 2017; published 24 August 2017)

$Cu_xBi_2Se_3$ is known for superconductivity due to Cu intercalation in the van der Waals gaps between the quintuple layers of $Bi_2Se_3$ at $x > 0.10$. Here we report the synthesis and transport properties of Cu-doped $Cu_xBi_2Se_3$ films prepared by the chemical-vapor-deposition (CVD) method with $0.11 \geqslant x \geqslant 0$. It is found that the insulatinglike temperature-dependent resistivity of polycrystalline $Cu_xBi_2Se_3$ films exhibits a marked metallic downturn and an increase of carrier concentration below ~37 K. There is also a time-dependent slow relaxation behavior in the resistance at low temperature. These effects might be related to the strong hybridization between $Cu^+$ and $Cu^{2+}$ conduction bands from the intercalated $Cu^+$ and substituted $Cu^{2+}$ sites in $Bi_2Se_3$ films. The findings here have important implications for the understanding and development of doping-induced superconductivity in topological insulators.

DOI: 10.1103/PhysRevB.96.075152

## I. INTRODUCTION

A topological insulator is a material that has a bulk electronic band gap and gapless edge states for charges and spins, which are protected by time-reversal symmetry [1,2]. The three-dimensional (3D) topological insulator $Bi_2Se_3$ has the simplest Dirac cone surface spectrum and the largest band gap (0.3 eV) [3]. Bulk $Bi_2Se_3$ has a lot of native defects, including the Se vacancy ($V_{Se}$) and the Bi antisite ($Bi_{Se}$), which result in that the bulk carriers from defects are dominant over the surface carriers and give rise to its *n*-type conductivity [4]. The surface chemical potential and the bulk Fermi level of $Bi_2Se_3$ can be tuned by chemical doping. By doping Mn [5], Ca [6], Cd [7], or codoping Sb and Pb [8], the carrier type of $Bi_2Se_3$ can be tuned from *n* type to *p* type. Especially in $Cu_xBi_2Se_3$, Cu not only compensates $Bi_2Se_3$ native defects and reduces the bulk carrier density [9,10], but also intercalates into the van der Waals gaps between Se layers [11]. Superconductivity has been observed in $Bi_2Se_3$ by Cu [11] or Sr [12,13] doping, which are promising candidates for topological superconductor (TSC) research. In $Cu_xBi_2Se_3$ with $x > 0.1$, topological order [14], quantum oscillations (the de Haas–van Alphen effect) [15], quantum anomalous thermal Hall effect [16], spin-rotation symmetry breaking [17], and odd-parity nematic superconductivity [18] have been observed, providing evidence that $Cu_xBi_2Se_3$ is a TSC, and opening up opportunities to realize Majorana fermions. However, there is very limited study on low Cu-doped $Cu_xBi_2Se_3$ ($x < 0.1$). In $Cu_xBi_2Se_3$ superconductors where $x > 0.1$, Cu primarily intercalates between Se layers [11,19–21]. The origin of the superconductivity in $Cu_xBi_2Se_3$ has been studied by many researchers. The tunneling spectrum of $Cu_{0.2}Bi_2Se_3$ shows that the density of states at the Fermi level is fully gapped without any in-gap states, being consistent with the Bardeen-Cooper-Schrieffer theory, which suggests that $Cu_{0.2}Bi_2Se_3$ is a classical *s*-wave superconductor [22]. This contradicting result might be reconciled by considering the evolution of the Fermi surface with carrier concentration [23] and the Dirac fermion states on the surface [24]. A subtle balance between two competing processes of electron and hole doping from Cu in $Cu_xBi_2Se_3$ single crystal was reported to be responsible for its superconductivity [21], and the disorder and inhomogeneity effects in $Cu_xBi_2Se_3$ film were reported to suppress the superconductivity [25]. It was known that Cu atoms can not only intercalate into the van der Waals gaps as $Cu^+$ state and donate electrons to $Bi_2Se_3$, but also substitute for Bi as $Cu^{2+}$ state and act as an acceptor [26–28]. Recently, angle-resolved photoemission spectroscopy (ARPES) results indicated that when Cu concentration is at a low level ($x < 0.05$), Cu predominantly intercalates into the van der Waals gap, while with further doping, Cu will replace Bi, causing the saturation of the carrier concentration [21]. Similar results were also obtained earlier by the reflectivity in infrared spectral region [26]. In addition to the two competing carrier doping effects and the disorder effect, the interaction of intercalated $Cu^+$ and substituted $Cu^{2+}$ also plays an important role in the electrical transport property. Superconductinglike behavior has been observed in the layered chalcogenides CuS and CuSe when temperature is below 40 K due to a strong hybridization between $Cu^+$ and $Cu^{2+}$ [29,30]. It has been noted that the conduction bands between two different site occupations of Cu in CuS take place a strong hybridization at low temperatures, resulting in the charge delocalization between these ions [30]. This behavior of CuS and CuSe is highly supported by two chemical characteristics: two-dimensional structure and mixed valence of copper [29]. $Bi_2Se_3$ has a layered structure consisting of Se(1)-Bi-Se(2)-Bi-Se(1) quintuple layers (QLs), and it is bonded by weak van der Waals force between QLs [31]. It has a rhombohedral crystal structure [space group $D_{3d}^5$ ($R\bar{3}m$)], with $a = 4.14$ Å and $c = 28.54$ Å [25]. It is similar to CuS (or CuSe) crystal structure (space group $P6_3/mmc$, layered structure), with $a = 3.7938$ Å and

*zhwang@imr.ac.cn
†zdzhang@imr.ac.cn

 

$c = 16.341$ Å [32,33]. Therefore, it would be interesting to see in Cu-doped $Bi_2Se_3$, whether a strong hybridization will occur between the intercalated $Cu^+$ in quintuple layers and the $Cu^{2+}$ substituting for $Bi^{3+}$ at low temperatures.

Here, Cu-doped $Bi_2Se_3$ polycrystalline thin films were prepared by the CVD method. It is found that the resistivity of the films changes from metallic in undoped samples to a nonmetallic behavior upon Cu doping, and a resistivity abnormality is observed at 37 K in the films with high Cu concentration, which is independent of the application of a magnetic field. We show that Cu atoms occupy both intercalated $Cu^+$ and substituted $Cu^{2+}$ sites in $Bi_2Se_3$ films by Raman spectroscopy. We suggest that the metallic downturn in the temperature-dependent resistivity and the carrier concentration increase at 37 K are due to a strong hybridization between the $Cu^+$ and $Cu^{2+}$ conduction bands and the electron delocalization accompanying it. There is also a time-dependent relaxation behavior in electrical transport at low temperature, which is attributed to the electron delocalization.

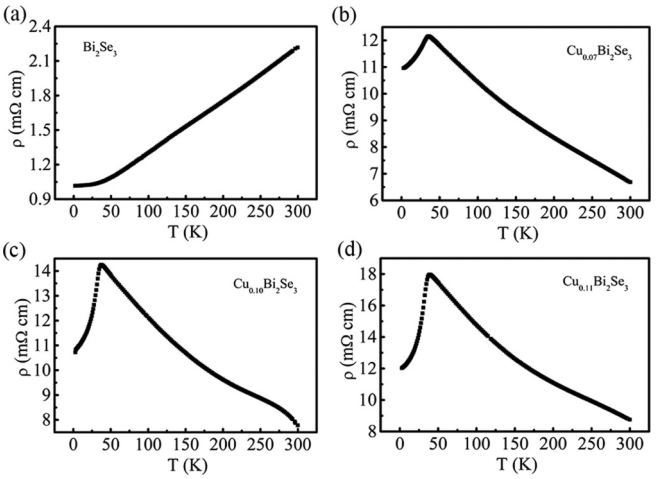


FIG. 1. Resistivity plotted as a function of temperature for four representative $Cu_xBi_2Se_3$ thin-film samples with respective $x = 0$, 0.07, 0.10, and 0.11, shown as (a), (b), (c), and (d).

## II. EXPERIMENT

Cu-doped $Bi_2Se_3$ films were grown by the CVD method on semiconductor Si substrates (with a thin amorphous $SiO_2$ layer on the surface) with size of ~1.5 cm × 1.5 cm in $H_2$/Ar carrier gas with flow ratio of 10/40 sccm. Briefly, a high-temperature tube furnace (Lindberg Blue M) and a quartz tube of 1 in. diameter were used as the reactor for the synthesis with accurate control of temperature and carrier gas flow rate. 99.99% $Bi_2Se_3$ powder and 98.5% $C_{10}H_{14}CuO_4$ powder were used as precursor. The $C_{10}H_{14}CuO_4$ powder has a low sublimation and decomposition temperature, and works as a convenient source for Cu vapor. They were placed, respectively, at a distance of 2 and 12–18 cm upstream from the center of the furnace at 520 °C. The Cu concentration can be controlled by the distance between the center of the furnace and the raw material of $C_{10}H_{14}CuO_4$ which determines the source temperature. The growth substrate was placed at a distance of 14–15 cm downstream from the center of the furnace. The pressure was kept at 24–30 Pa for 5 min to deposit the Cu-doped $Bi_2Se_3$ film. After that, the tube furnace was cooled naturally down to room temperature, and a dark-gray Cu-doped $Bi_2Se_3$ film was found on the Si substrates.

The phase structure of the Cu-doped $Bi_2Se_3$ films was confirmed by x-ray diffraction (XRD) using a Bruker D8 diffractometer with Cu $K\alpha$ radiation. The analyses on the morphology and composition of samples were performed by field emission scanning electron microscopy (FESEM) and energy dispersive x-ray spectroscopy (EDS or EDX) (JSM 6301F). The site occupancies of Cu atoms in $Bi_2Se_3$ were checked by a Renishaw inVia Raman spectrometer equipped with a 633 nm excitation laser (17 mW). Transport properties were measured in a physical property measurement system (PPMS, Quantum Design). Samples were cut into a shape with length about 1 cm and width of 3-4 mm. The resistivity versus temperature measurements were performed using a standard four-probe technique with silver paste as contacts. The Hall resistance versus temperature and magnetic field curves were collected with the Hall bar configuration.

## III. RESULTS AND DISCUSSION

The temperature-dependent resistivity ($R$-$T$) of $Cu_xBi_2Se_3$ films were investigated in the temperature range from 300 to 2 K at zero magnetic field. The $R$-$T$ curves of these four samples with respective $x = 0, 0.07, 0.10$, and 0.11 are shown in Fig. 1. The Cu concentrations of all samples are determined by EDS measurements. The undoped $Bi_2Se_3$ film shows metallic $R$ vs $T$ [Fig. 1(a)] which is similar to previous reports [34–36]. The high-temperature behavior of resistivity changes from metallic to a nonmetallic insulatinglike behavior with Cu doping in $Cu_xBi_2Se_3$ films, as shown in Fig. 1. However, we found that the resistivity shows a sharp drop at ~37 K at Cu concentration $x > 0.066$, as shown in Figs. 1(b)–1(d) and Fig. S1 in Ref. [37]. This phenomenon (a sharp decrease in the resistivity) has never been reported in $Cu_xBi_2Se_3$. More results of other samples with different Cu concentrations are represented in Fig. S1 in the Supplemental Material [37]. The thin films are grown on Si substrate with a thin amorphous $SiO_2$ layer (about 10 nm by natural oxidation), as shown in Fig. S2. There is the van der Waals force between the thin film and the substrate. It is indicated that no epitaxial strain exists in these films, so the epitaxial strain does not play a crucial role in the sharp drop in resistivity at ~37 K. From Fig. S1, we note that the metal-insulator transition temperature is almost the same with $x$ increasing from 0.07 to 0.11. In order to understand the annealing effect on transport properties of films, the prepared $Cu_xBi_2Se_3$ ($x = 0.068$ and 0.071) thin films were annealed at 573 K (the temperature that Cu-doped $Bi_2Se_3$ thin films were deposited on substrates) for 5 h. The $R$-$T$ properties of the prepared thin films with and without annealing were measured. As shown in Fig. 2, we can see that the decreasing amplitudes ($[\rho_{(37\,K)} - \rho_{(2\,K)}]/[\rho_{(37\,K)} - \rho_{(300\,K)}]$) of two $R$-$T$ curves before and after annealing do not show much difference, indicating that Cu in prepared $Cu_xBi_2Se_3$ thin film has a homogeneous distribution.

Figures 3 and S3 (see Fig. S3 in Ref. [37]) show the scanning electron microscopy (SEM) images of typical samples. The thickness of all thin films can be estimated from the SEM images of samples taken from the side view [SEM images shown

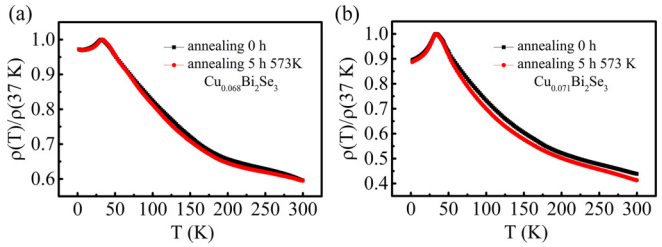


FIG. 2. Temperature dependence of resistivity of (a) $Cu_xBi_2Se_3$ ($x = 0.068$) and (b) $Cu_xBi_2Se_3$ ($x = 0.071$) before (black square) annealing and after (red circle) annealing at 573 K for 5 h.

in Fig. S3(d)], which are 300 ± 20 nm. Figure 3(a) is a typical SEM image of synthesized (undoped) $Bi_2Se_3$ film, showing interconnected grains of $Bi_2Se_3$ nanoplates. Figures 3(b)–3(d) are the SEM images of $Cu_xBi_2Se_3$ films with $x = 0.07$, 0.10, and 0.11. First, it is clear that the size of (undoped) $Bi_2Se_3$ nanoplates is bigger than that of $Cu_xBi_2Se_3$. Moreover, with Cu doping, not only the lateral size of nanoplates along the *ab* plane becomes smaller; there are also more vertically grown nanoplates which likely cause stronger scattering in doped $Cu_xBi_2Se_3$ films and the nonmetallic $R$ vs $T$ between 37 and 300 K. It is similar to the nonmetallic behavior in $Bi_2Te_3$ films [38] grown by the CVD method, which is attributed to the structural disorder and porosity. However, the effect of the size of nanoplates cannot cause the sudden metallic downturn at 37 K in our films. A similar nonmetallic behavior is observed in the granular metals [39], which are arrays of metallic particles embedded into an insulating matrix. But the periodic granular array model [39] is different from the continuous film and the critical conductance theory of metal-insulator transition is not applicable to our case. In order to exclude Cu clusters effect in Cu-doped $Bi_2Se_3$ thin film, the EDX element mappings were measured to observe the element distribution of the Cu-doped $Bi_2Se_3$ thin-film sample ($x = 0.071$). As shown in Fig. S4 of

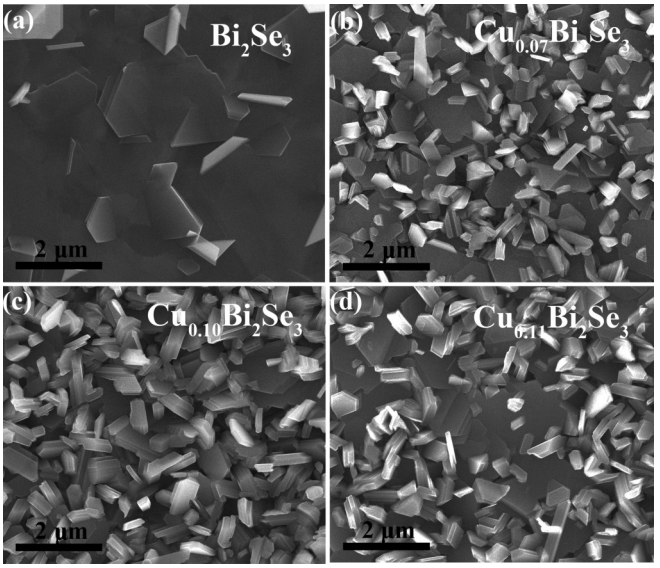


FIG. 3. SEM images of $Cu_xBi_2Se_3$ films with different Cu concentration. (a) An undoped sample ($x = 0$). (b) A sample with $x = 0.07$, (c) a sample with $x = 0.10$, and (d) a sample with $x = 0.11$.

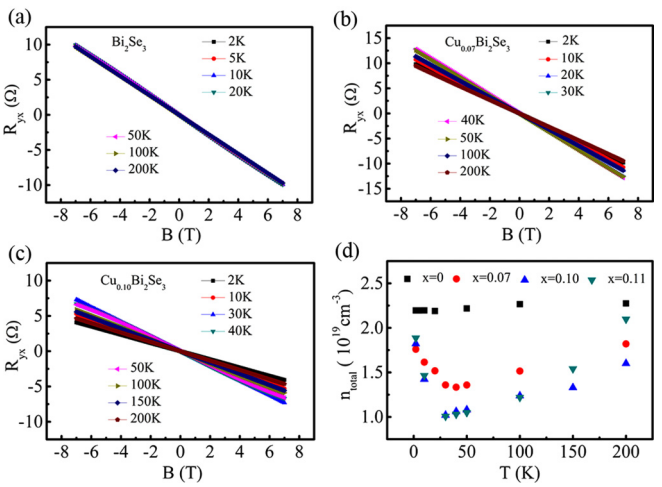


FIG. 4. Hall resistance data of $Cu_xBi_2Se_3$ thin-film samples. (a) An undoped sample ($x = 0$). (b) A sample with $x = 0.07$ and (c) a sample with $x = 0.10$. (d) Total carrier concentration of four typical samples ($x = 0$, 0.07, 0.10, and 0.11) as a function of temperature.

the Supplemental Material [37], we find that the Cu atoms in thin films have a homogeneous distribution.

Figures 4(a)–4(c) show the Hall resistance $R_{yx}$ as a function of $B$ (perpendicular magnetic field) at various temperatures for samples with $x = 0$, 0.07, and 0.10. The sign of $R_{yx}$ of all samples indicates $n$-type conduction. Figure 4(a) illustrates that the $R_{yx}$ of undoped samples is almost independent of temperature. Figures 4(b)–4(c) show that $R_{yx}$ of doped $Cu_xBi_2Se_3$ samples is temperature dependent, and the temperature dependence becomes more pronounced with increasing Cu concentration. Additional Hall resistances for more samples are shown in Fig. S5 of the Supplemental Material [37]. We use the high field slope of $R_{yx}(B)$, i.e., $dR_{yx}/dB$ to extract $n_{\text{total}}$, the total carrier concentration. The total carrier concentrations for the four typical samples with $x = 0$, 0.07, 0.10, and 0.11 are presented in Fig. 4(d). The $n_{\text{total}}$ is on the order of $10^{19}/\text{cm}^3$ for all the samples. We found that the carrier concentration variation with temperature is interesting. For undoped samples, carrier concentration is hardly affected by temperature. The carrier concentration is almost unchanged with temperature decreasing from 200 to 2 K. In Cu-doped samples, the carrier concentration first decreases with lowering the $T$, and then increases at temperatures lower than about 37 K. The variation of carrier concentration is concomitant with the kink in $R$ vs $T$, suggesting a common origin for both phenomena.

In order to study the effect of Cu doping in $Bi_2Se_3$, the structure and composition of these samples were investigated by XRD and EDS. XRD patterns of all samples show pure $Bi_2Se_3$-type structure. As shown in Fig. 5(a), most of the reflections are strong along the $c$-axis oriented (00$l$) tropism in the undoped sample, which consists of the SEM image, reflecting that the (undoped) $Bi_2Se_3$ film displays a continuous film with triangular or hexagonal flakes laying on the substrate. Figure 5(a) also shows that the doped $Cu_xBi_2Se_3$ samples are polycrystalline without oriented (00$l$) tropism. The lattice parameters are calculated by XRD analysis software MDI JADE 5.0 from the XRD patterns. Table I lists the lattice constants $a$ and $c$ obtained by XRD, and Cu concentrations obtained by

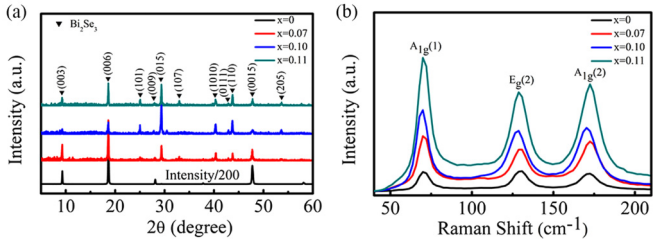


FIG. 5. (a) XRD patterns of $Cu_xBi_2Se_3$ thin-film samples with respective $x = 0$, 0.07, 0.10, and 0.11. (b) Raman spectra of the four samples in (a).

EDS for four samples with different $x$. From Table I, we find that Cu doping causes the monotonic increase of the $c$-axis length. It suggests that Cu atoms are intercalated into the van der Waals gaps between QLs of $Bi_2Se_3$. Moreover, Cu doping also leads to a slight decrease in the lattice along the $a$ axis, compared with that of (undoped) $Bi_2Se_3$, due to the fact that Cu randomly substitutes for Bi within the host structure, as shown in Table I. However, the lattice constant $a$ is almost the same in samples with $x$ from 0.07 to 0.11, suggesting that the difference in the lattice constant $a$ is not significant in this Cu concentration range.

Figure 5(b) presents Raman spectra for $\lambda = 633$ nm excitation at 295 K. When Cu intercalates between the QLs of $Bi_2Se_3$, both peaks of the bulk phonon modes [$E_g(2)$ and $A_{1g}(2)$] will shift to lower frequencies [40,41]. However, $E_g(2)$, $A_{1g}(1)$, and $A_{1g}(2)$ modes are expected to shift to higher frequencies when Bi is substituted by other small atoms [42]. High-frequency modes are out-of-phase movements of the outer Bi and Se atoms which are attracted by the strongest bonding forces in the crystals [42]. Therefore, interactions between the QLs are weakened by the intercalation of Cu atoms and the substitution of Cu atoms strengthens the interlayer van der Waals forces. As shown in Fig. 5(b), the $A_{1g}(1)$ mode peak does not shift clearly with increasing Cu concentration due to its low-frequency nature. The $E_g(2)$ and $A_{1g}(2)$ mode peaks first shift to lower frequencies at low Cu concentrations, and then shift to higher frequencies with further increasing Cu concentration. It indicates that Cu atoms occupy the intercalative sites between the QLs at low Cu concentrations, and take the substitutional sites of Bi atoms gradually with increasing Cu concentration, which is similar to the previous report [21]. These findings confirm that the substitution Cu and the intercalation Cu atoms are both present in $Cu_xBi_2Se_3$ polycrystalline thin films. When Cu intercalates into the van der Waals gap, it can donate an electron to $Bi_2Se_3$ as the $Cu^+$ state, and the substituted Cu is in the $Cu^{2+}$ state and acts as an acceptor [26–28].

TABLE I. Lattice constants $a$ and $c$, and the Cu concentration in $Cu_xBi_2Se_3$ thin-film samples obtained by XRD and EDS.

| | $a$ (Å) | $c$ (Å) | Doping level $x$ |
|---|---|---|---|
| Sample 1 | 4.152 ± 0.002 | 28.54 ± 0.01 | 0 |
| Sample 2 | 4.135 ± 0.002 | 28.55 ± 0.01 | 0.07 |
| Sample 3 | 4.135 ± 0.002 | 28.60 ± 0.01 | 0.10 |
| Sample 4 | 4.136 ± 0.002 | 28.64 ± 0.01 | 0.11 |

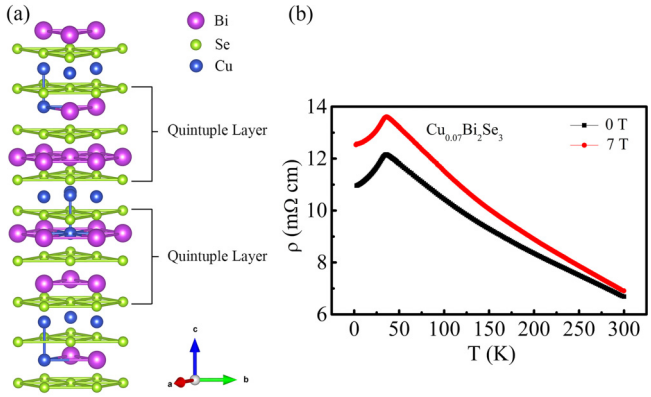


FIG. 6. (a) Crystal structure of Cu-doped $Bi_2Se_3$, including both intercalated Cu and substitutional Cu. (b) The temperature-dependent resistivity of a $Cu_xBi_2Se_3$ ($x = 0.07$) thin film with an applied magnetic field of 7 T and zero field.

By analogy of other similar layered selenides [29], we infer a structural diagram of $Cu_xBi_2Se_3$ with both intercalated Cu sites and random substitutional Cu sites, as schematically shown in Fig. 6(a). In our work, Cu is also found to randomly substitute for Bi within the host structure, which differs from the bulk $Cu_xBi_2Se_3$ single crystals reported with superconductor phase, suggesting that the site occupancy of Cu in $Bi_2Se_3$ depends on the process of sample growing [11].

As known, strong hybridization between the adjacent $Cu^+$ and $Cu^{2+}$ conduction bands takes place at low temperature, as observed in the 2D regime of CuS and CuSe [29,30]. It indicates that charge delocalization between these ions can occur in the 2D regime [29]. As shown in Fig. 4(d), the carrier concentration of $Cu_xBi_2Se_3$ thin films increases significantly below 37 K, which probably originates from the delocalized electrons by the strong hybridization between adjacent $Cu^+$ and $Cu^{2+}$ conduction bands. This scenario appears to be compatible with the resistivity drop at 37 K, as shown in Figs. 1(b)–1(d). One may suspect that these features come from the CuSe phase due to the superconductinglike property of CuSe. To address this possibility, we studied the effect of magnetic field and ruled it out since the superconductinglike behavior of CuSe is sensitive to magnetic field (such as 7 T) [29]. We compare the $R$-$T$ behaviors of $Cu_xBi_2Se_3$ ($x = 0.07$) in zero field vs a magnetic field of 7 T, as shown in Fig. 6(b). The kink of $R$ vs $T$ at 37 K does not change, but there is a magnetoresistance. More data are shown in Fig. S6 of the Supplemental Material [37]. This positive magnetoresistance is a normal phenomenon in topological insulators, such as in $Bi_2Se_3$ [43], $Bi_2Te_3$ [38], and nonmagnetic Sn-doped $Bi_2Te_3$ film [44]. Furthermore, we measured the current-voltage ($I$-$V$) curves of two representative samples with $x = 0.10$ and 0.11 by using the current value far smaller than the one used in the $R$-$T$ curves. Both of them show linear $I$-$V$ characteristics at 2 K, 50 K below and above 37 K (see Fig. S7 in Ref. [37]). These are not the characteristics expected for superconductors. The effect of the structural phase transition is excluded by a temperature-dependent x-ray diffractometer using Empyrean PIXcel 3D produced by PANalytical. We measured the XRD patterns of a typical sample ($x = 0.081$) at 20, 50, and 298 K, respectively

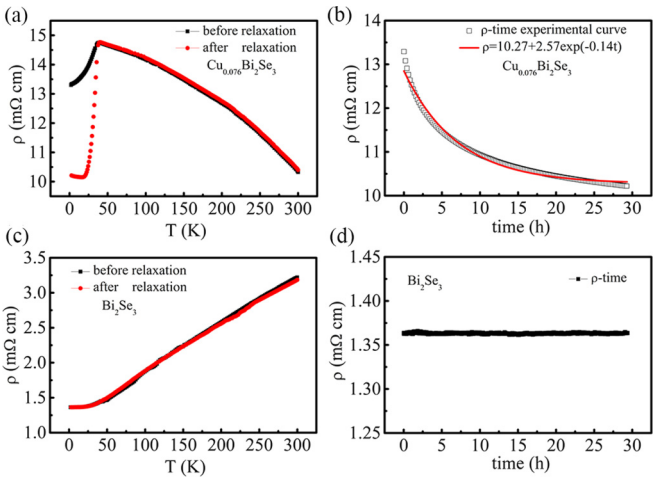


FIG. 7. Temperature dependence of resistivity of (a) $Cu_xBi_2Se_3$ ($x = 0.076$) and (c) undoped $Bi_2Se_3$ before (black square) and after (red circle) relaxation at 2 K for 29 h. Time dependence of resistivity of (b) $Cu_xBi_2Se_3$ ($x = 0.076$) and (d) undoped $Bi_2Se_3$ at 2 K for the relaxation process of 29 h.

(see Fig. S8 in Ref. [37]). It is noted that the sample was kept at 20 K for 2 h to stabilize the phase before measurement. The kink is observed in the *R-T* curve at about 37 K [see Fig. S8(a) in Ref. [37]]. As shown in Fig. S8(b) of the Supplemental Material [37], there is no indication for structural phase transition at 37 K. With decreasing temperature, all peaks in the XRD spectrum shift to higher angles with a small range, which indicates that its lattice constants exhibit a slight decrease at low temperature. These results indicate that our case is different from the superconductinglike behavior in CuSe and there is no structural phase transition around 37 K; a more likely explanation is the strong hybridization between the adjacent $Cu^+$ and $Cu^{2+}$ conduction bands in Cu-doped $Bi_2Se_3$ polycrystalline thin film, which causes the electron delocalization.

Further study reveals that a time-dependent relaxation phenomena is in electronic transport at low temperature. Figure 7(a) shows the temperature dependence of resistivity at zero magnetic field of $Cu_xBi_2Se_3$ ($x = 0.076$) before and after relaxation at 2 K. The *R-T* curve (black squares) was measured with decreasing temperature from 300 to 2 K, and then the sample was kept at 2 K for 29 h without any external excitation. Then the resistivity (red circles) was measured with increasing temperature from 2 to 300 K, as shown in Fig. 7(a). From Fig. 7(a), it is noted that the kink of resistivity at 37 K is more pronounced after the sample is allowed to stabilize at low temperature for a long time and the two resisvivity curves do not show much deviation above 37 K. As it is unlikely that the thermal contact between the sample and enviornment suddenly changes at 37 K, these data exclude the poor thermalization (or thermal contact) of the sample as the explanation for the relaxation phenomenon below 37 K.

Although the exact mechanism of the slow dynamics observed below 37 K remains unknown, we performed more characterizations to gain further understanding. Figure 7(b) shows the resistivity relaxation process with time at 2 K. The red line is the fitting curve to the following formula [45,46]:

$$\rho(t) = \rho(\infty) + [\rho(0) - \rho(\infty)]\exp(-Et), \qquad (1)$$

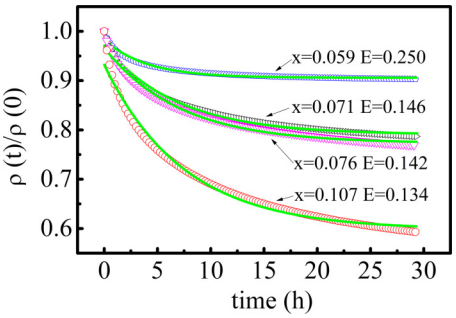


FIG. 8. Time dependence of resistivity at 2 K for different Cu concentrations of $Cu_xBi_2Se_3$ ($x = 0.059$, 0.071, 0.076, and 0.107). Solid lines (green) are best fits to formula (1): $\rho_{(t)}/\rho_{(0)} = \rho_{(\infty)}/\rho_{(0)} + [\rho_{(0)} - \rho_{(\infty)}]/\rho_{(0)}\exp(-Et)$.

where $t$ is the relaxation time, $\rho_{(0)}$ is the initial resistivity, $\rho_{(t)}$ is the time-dependent resistivity, $\rho_{(\infty)}$ is the saturation resistivity, and $E$ is the relaxation rate. More data on additional samples are given in Fig. S9 of the Supplemental Material [37]. For comparison, the temperature-dependent resistivity and relaxation behavior of the undoped $Bi_2Se_3$ film are shown in Figs. 7(c) and 7(d), respectively. The time-dependent slow relaxation behavior is clearly absent in the undoped $Bi_2Se_3$ film. In addition, the dependence of resistivity vs time at 2 K for $Cu_xBi_2Se_3$ films with different Cu concentrations is shown in Fig. 8. When the Cu concentration increases, the relaxation rate $E$ decreases (relaxation becomes slower). Meanwhile, the magnetitude of the resistivity change during relaxation also increases at higher doping level, accompanying the slower relaxation dynamics.

## IV. CONCLUSION

In conclusion, we have performed a structure and transport property study of $Cu_xBi_2Se_3$ polycrystalline thin films with $0.11 \geqslant x \geqslant 0$ prepared by the CVD method. Raman analysis shows that there are both intercalated $Cu^+$ and substituted $Cu^{2+}$ in $Cu_xBi_2Se_3$. Due to disorder, Cu-doped $Bi_2Se_3$ polycrystalline thin films exhibit nonmetallic temperature-dependent resistivity between 37 and 300 K. However, an unexpected sign change in $dR/dT$ is observed at 37 K. It is suggested that the hybridization effect between $Cu^+$ and $Cu^{2+}$ conduction bands is responsible for the metallic behavior at $T < 37$ K. Moreover, a relaxation behavior was observed in the time dependence of resistivity in the metallic state below 37 K, calling for the further understanding of the dynamics in $Cu_xBi_2Se_3$ polycrystalline thin films.

## ACKNOWLEDGMENTS

This work was supported by the National Natural Science Foundation of China (Grants No. 51522104 and No. 51331006) and the National Key R&D Program of China (Grant No. 2017YFA0206302). X.P.A.G. thanks the National Science Foundation (DMR-1151534) for financial support. Q.R.Y. and G.H.R. acknowledge the financial support of Guangxi National Science Foundation (Grant No. 2012GXNSFGA060002).

[1] C. L. Kane and E. J. Mele, Phys. Rev. Lett. **95**, 146802 (2005).
[2] M. Konig, S. Wiedmann, C. Brune, A. Roth, H. Buhmann, L. W. Molenkamp, X. L. Qi, and S. C. Zhang, Science **318**, 766 (2007).
[3] M. Z. Hasan and C. L. Kane, Rev. Mod. Phys. **82**, 3045 (2010).
[4] D. West, Y. Y. Sun, H. Wang, J. Bang, and S. B. Zhang, Phys. Rev. B **86**, 121201(R) (2012).
[5] Y. H. Choi, N. H. Jo, K. J. Lee, H. W. Lee, Y. H. Jo, J. Kajino, T. Takabatake, K. T. Ko, J. H. Park, and M. H. Jung, Appl. Phys. Lett. **101**, 152103 (2012).
[6] Y. S. Hor, A. Richardella, P. Roushan, Y. Xia, J. G. Checkelsky, A. Yazdani, M. Z. Hasan, N. P. Ong, and R. J. Cava, Phys. Rev. B **79**, 195208 (2009).
[7] Z. Ren, A. A. Taskin, S. Sasaki, K. Segawa, and Y. Ando, Phys. Rev. B **84**, 075316 (2011).
[8] Y. Zhang, C. Z. Chang, K. He, L. L. Wang, X. Chen, J. F. Jia, X. C. Ma, and Q. K. Xue, Appl. Phys. Lett. **97**, 194102 (2010).
[9] T. S. Chen, Q. Chen, K. Schouteden, W. K. Huang, X. F. Wang, Z. Li, F. Miao, X. R. Wang, Z. G. Li, B. Zhao, S. C. Li, F. Q Song, J. L Wang, B. G. Wang, C. V. Haesendonck, and G. H. Wang, Nat. Commun. **5**, 5022 (2014).
[10] M. Brahlek, N. Koirala, M. Salehi, N. Bansal, and S. Oh, Phys. Rev. Lett. **113**, 026801 (2014).
[11] Y. S. Hor, A. J. Williams, J. G. Checkelsky, P. Roushan, J. Seo, Q. Xu, H. W. Zandbergen, A. Yazdani, N. P. Ong, and R. J. Cava, Phys. Rev. Lett. **104**, 057001 (2010).
[12] Shruti, V. K. Maurya, P. Neha, P. Srivastava, and S. Patnaik, Phys. Rev. B **92**, 020506(R) (2015).
[13] C. Q. Han, H. Li, W. J. Chen, F. F. Zhu, M. Y. Yao, Z. J. Li, M. Wang, B. F. Gao, D. D. Guan, C. H. Liu, C. L. Gao, D. Qian, and J. F. Jia, Appl. Phys. Lett. **107**, 171602 (2015).
[14] L. A. Wray, S. Y. Xu, Y. Q. Xia, Y. S. Hor, D. Qian, A. V. Fedorov, H. Lin, A. Bansil, R. J. Cava, and M. Z. Hasan, Nat. Phys. **6**, 855 (2010).
[15] B. J. Lawson, Y. S. Hor, and L. Li, Phys. Rev. Lett. **109**, 226406 (2012).
[16] Y. Shimizu, A. Yamakage, and K. Nomura, Phys. Rev. B **91**, 195139 (2015).
[17] K. Matano, M. Kriener, K. Segawa, Y. Ando, and G. Q. Zheng, Nat. Phys. **12**, 852 (2016).
[18] S. Yonezawa, K. Tajiri, S. Nakata, Y. Nagai, Z. W. Wang, K. Segawa, Y. Ando, and Y. Maeno, Nat. Phys. **13**, 123 (2017).
[19] M. Kriener, K. Segawa, Z. Ren, S. Sasaki, S. Wada, S. Kuwabata, and Y. Ando, Phys. Rev. B **84**, 054513 (2011).
[20] M. Kriener, K. Segawa, Z. Ren, S. Sasaki, and Y. Ando, Phys. Rev. Lett. **106**, 127004 (2011).
[21] Y. Tanaka, K. Nakayama, S. Souma, T. Sato, N. Xu, P. Zhang, P. Richard, H. Ding, Y. Suzuki, P. Das, K. Kadowaki, and T. Takahashi, Phys. Rev. B **85**, 125111 (2012).
[22] N. Levy, T. Zhang, J. Ha, F. Sharifi, A. A. Talin, Y. Kuk, and J. A. Stroscio, Phys. Rev. Lett. **110**, 117001 (2013).
[23] E. Lahoud, E. Maniv, M. S. Petrushevsky, M. Naamneh, A. Ribak, S. Wiedmann, L. Petaccia, Z. Salman, K. B. Chashka, Y. Dagan, and A. Kanigel, Phys. Rev. B **88**, 195107 (2013).
[24] T. Mizushima, A. Yamakage, M. Sato, and Y. Tanaka, Phys. Rev. B **90**, 184516 (2014).
[25] T. Shirasawa, M. Sugiki, T. Hirahara, M. Aitani, T. Shirai, S. Hasegawa, and T. Takahashi, Phys. Rev. B **89**, 195311 (2014).
[26] A. Vasko, L. Tichy, J. Horak, and J. Weissenstein, Appl. Phys. **5**, 217 (1974).
[27] C. Martin, V. Craciun, K. H. Miller, B. Uzakbaiuly, S. Buvaev, H. Berger, A. F. Hebard, and D. B. Tanner, Phys. Rev. B **87**, 201201(R) (2013).
[28] Z. Liu, X. Y. Wei, J. J. Wang, H. Pan, F. H. Ji, F. C. Xi, J. Zhang, T. D. Hu, S. Zhang, Z. Jiang, W. Wen, Y. Y. Huang, M. Ye, Z. Q. Yang, and S. Qiao, Phys. Rev. B **90**, 094107 (2014).
[29] B. Raveau and T. Sarkar, Solid State Sci. **13**, 1874 (2011).
[30] R. R. Gainov, A. V. Dooglav, I. N. Pen'kov, I. R. Mukhamedshin, N. N. Mozgova, I. A. Evlampiev, and I. A. Bryzgalov, Phys. Rev. B **79**, 075115 (2009).
[31] Y. Xia, D. Qian, D. Hsieh, L. Wray, A. Pal, H. Lin, A. Bansil, D. Grauer, Y. S. Hor, R. J. Cava, and M. Z. Hasan, Nat. Phys. **5**, 398 (2009).
[32] H. T. Evans, Jr. and J. A. Konnert, Am. Mineral. **61**, 996 (1976).
[33] H. J. Gotsist, A. C. Barnes, and P. Strange, J. Phys.: Condens. Matter **4**, 10461 (1992).
[34] N. Bansal, Y. S. Kim, M. Brahlek, E. Edrey, and S. Oh, Phys. Rev. Lett. **109**, 116804 (2012).
[35] L. Xue, P. Zhou, C. X. Zhang, C. Y. He, G. L. Hao, L. Z. Sun, and J. X. Zhong, AIP Adv. **3**, 052105 (2013).
[36] S. Urazhdin, D. Bilc, S. H. Tessmer, and S. D. Mahanti, Phys. Rev. B **66**, 161306(R) (2002).
[37] See Supplemental Material at http://link.aps.org/supplemental/10.1103/PhysRevB.96.075152 for complementing data of more samples with SEM, TEM, XRD, and transport properties.
[38] Z. H. Wang, L. Yang, X. J. Li, X. T. Zhao, H. L. Wang, Z. D. Zhang, and X. P. A. Gao, Nano Lett. **14**, 6510 (2014).
[39] I. S. Beloborodov, A. V. Lopatin, V. M. Vinokur, and K. B. Efetov, Rev. Mod. Phys. **79**, 469 (2007).
[40] V. Gnezdilov, Y. G. Pashkevich, H. Berger, E. Pomjakushina, K. Conder, and P. Lemmens, Phys. Rev. B **84**, 195118 (2011).
[41] H. M. Yi, C. Y. Chen, X. Sun, Z. J. Xie, Y. Feng, A. J. Liang, Y. Y. Peng, S. L. He, L. Zhao, G. D. Liu, X. L. Dong, J. Zhang, C. T. Chen, Z. Y. Xu, G. D. Gu, and X. J. Zhou, Chin. Phys. Lett. **32**, 067401 (2015).
[42] W. Richter, H. Kohler, and C. R. Becker, Phys. Status Solidi B **84**, 619 (1977).
[43] J. Wang, A. M. DaSilva, C. Z. Chang, K. He, J. K. Jain, N. Samarth, X. C. Ma, Q. K. Xue, and M. H. W. Chan, Phys. Rev. B **83**, 245438 (2011).
[44] H. B. Zhang, H. L. Yu, D. H. Bao, S. W. Li, C. X. Wang, and G. W. Yang, Adv. Mater. **24**, 132 (2012).
[45] S. Anghel, A. Singh, F. Passmann, H. Iwata, J. N. Moore, G. Yusa, X. Q. Li, and M. Betz, Phys. Rev. B **94**, 035303 (2016).
[46] W. F. Marashdeh, J. Longun, and J. O. Iroh, J. Appl. Polym. Sci. **133**, 43684 (2016).